SUPPORTING INFORMATION

Appendix

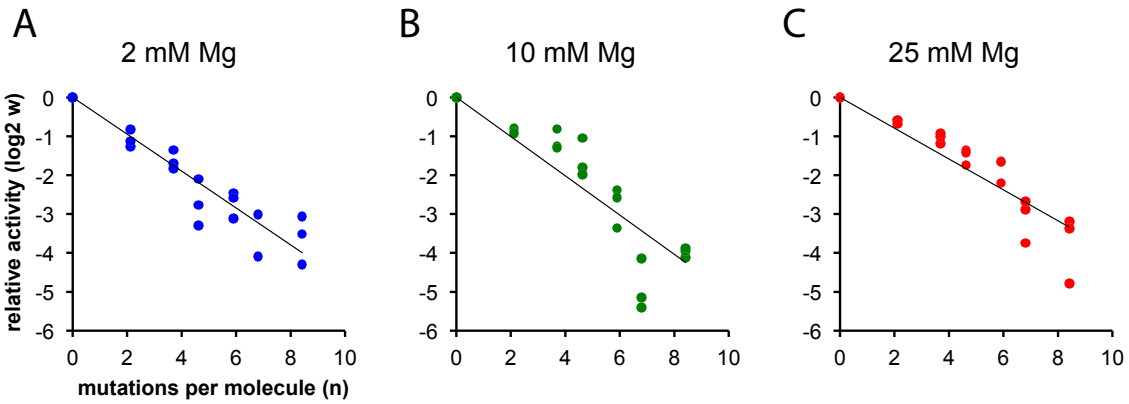

Figure S1 **Log transformations of fitness decline data.** Population fitness *w* (relative activity) was $\log_2$ transformed, and then fit by linear regression. This semi-log treatment is equivalent to a pure exponential (no epistasis) treatment of non-transformed data as in Fig. 3A of the main text, but helps highlight systematic deviations. The data demonstrates that this no epistasis treatment gives a reasonable fit to the stressful data (A, 2 mM $MgCl_2$, blue), but does not fit well to the data obtained at intermediate (B, 10 mM $MgCl_2$, green) or relaxed conditions (C, 25 mM $MgCl_2$, red). For these less stressful environments (B and C) the population fitness data is consistently higher than the curve predicts for lower numbers of mutations per molecule (n<6). This was the motivation for the epistatic treatment in the main text.

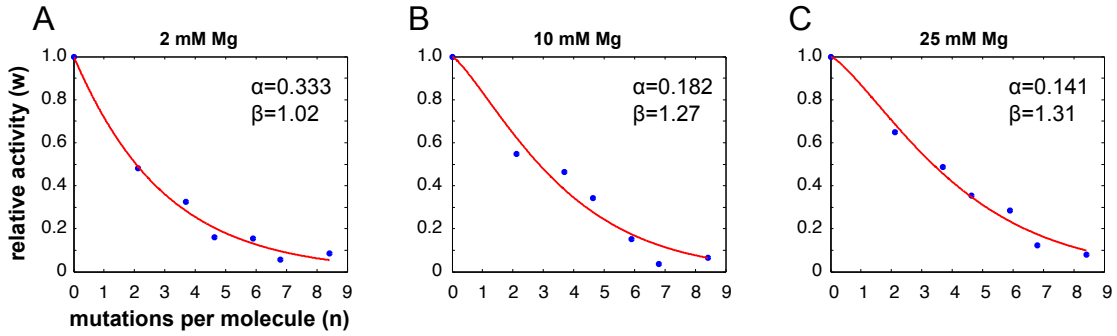

Figure S2 **Non-linear curve fitting used to extract parameters *α* and *β*.** To account for epistatic interactions, the equation $w(n)=\exp(-\alpha n^{\beta})$ was fit to the activity decline data from each chemical environment using non-linear curve fitting (Matlab). Curves were fit to three biological replicates, each blue data point shows the mean activity of the replicates. The fitting parameters of each red curve are shown within each plot.

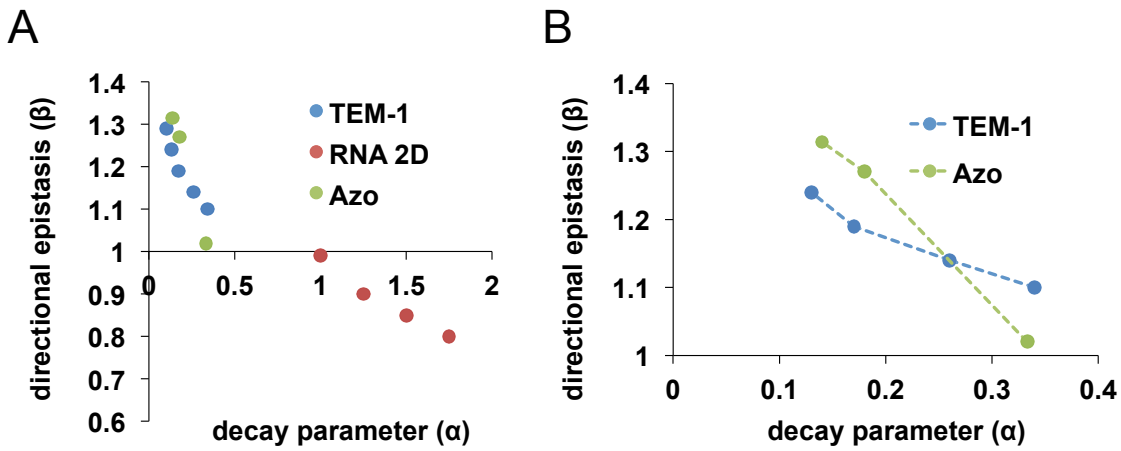

Figure S3 **Comparison of *Azoarcus* ribozyme data to previous reports on average deleterious mutational effects and epistasis.** *(A)* The previously reported *α* and *β* parameters for computationally predicted RNA secondary structures (RNA 2D, red) and the TEM-1 protein (blue) are plotted along with our current *Azoarcus* ribozyme results for comparison purposes only. The values for computationally folded RNA[33,35] secondary structures and the TEM-1 protein were approximated from the figures in the literature. For the TEM-1 values please see the Supplementary Information for Bershtein et al. (2006) *Nature* 444:929-932. *(B)* The values for the TEM-1 protein and the *Azoarcus* ribozyme are re-plotted to facilitate comparison.

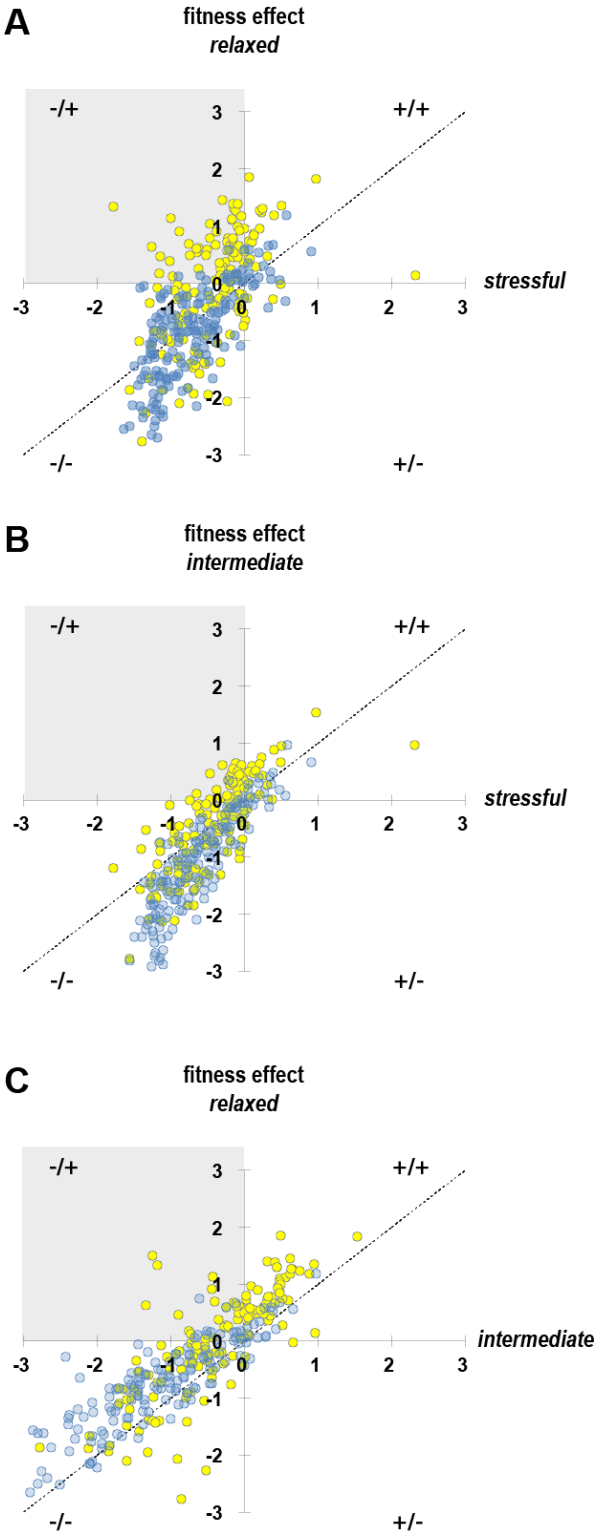

Figure S4 **Scatter plots of fitness effects.** Each data point represents a specific nucleotide substitution at a specific position in the ribozyme sequence (see Fig. 2 in main text). The "fitness effect" for each mutation is determined by the change in the relative frequency of the mutation following selection. It is defined as w = [frequency after selection]/[frequency before selection]. Each plot illustrates the correlation between the fitness effect under two different conditions; *stressful* (*2 mM* $MgCl_2$), *intermediate* (*10 mM* $MgCl_2$), *and relaxed* (*25 mM* $MgCl_2$) The data from the higher stress environment (lower magnesium concentrations) is always on the x-axis. The result is that the gray quadrant highlights a region where the same mutation is enriched at higher magnesium but deleterious or neutral at lower magnesium. The "-/+" symbol indicates that the data in that quadrant is less than zero (-) for x, and greater than zero (+) for y. As expected, the most extreme comparison (A) between relaxed vs. stressful conditions shows the greatest number of data points in this grey region of interest. The dashed diagonal line is for reference only (slope = 1) and is not a fit to the data.

Seq ID	Sequence	Selection [$MgCl_2$]
E27-1	GUGCCUUGCGCCGGGAAACCACGCAAGGGAUGGUGUCAAAUUCGGCGAAACCUAAGCG CCCGCCCGGGCGUAUGGCAACGCGGAGCCAAGCUUCGGCGCCUGCGCCGAUGAAGGUG UAGCGACUAGACGGCACCCACCUAAGGCAAACGCUAUGGUGAAGGCAUAGUCUAGGGA GUGGCGAAAGUCACACAAACCGG	25
E27-15	GUGCCUUGCGCCGGGAAACCACGCAAGGGAUGGUGUCAAAUUCGGCGAAACCUAAGUG CCCACCCGGGCGUAUGGCAACGCCGAGCCAAGCUUCGGCGCCUGCGCCGAUG–AGGCGU AGAGACUAGACGGCACCCACCUAAGGCGAACGCUAUGGUGAAGGCUUAGUCCAGGGAG UGGCGAAAGUCACACAAACCGG	25
E27-6	GUGCCUUGCGCCGGGAAACCACGCAAGGGAUGGUGUCAAAUUCGGCAAAACCUAAGCG CCCGCCCGGGCGUAAGGCAACGCCGAGCCAAGCUUCGGCGCCUGAGCCGACGAAGGUGU AGAGACUAGACGGCACCCACCUAAGGCAAACGCUAUGGUGAUGGCAUAGUCCAGGGAG UGGCGAAAGUCACACAAACCGG	25
E27-12	GUGCCUUGCGCCGGGAAACCACGCAAGGGAUGGUGUCAAAUUCGGCGAAACCUAAGCG CCCGCCCGGGCGUAUGGCAACGCCGAGCCAAGCUUCGGCGCCUGCGCCGAUGGAGGUG UAGAGACUAGAACGGCACCCACCUAAGGCAAACGUUAUGGUGAAGGCAUAGUCCAGGG AGUGGCGAAAGUCACACAAACCGG	25
E27-16	GUGCCUUGCGCCGGGAAACCACGCAAGGGAUGGUGUCAAAUUCGGCGAAACCUAAGCG CCCUCCCGGGCGUAUGGCUACGCCGAGCCAAGCUUUCGGCGCCUGCGCCGAUGAAGGU GUAGAGACUUGACGGCACCCACCUAAGGCAAACGCUAUGGUGAUGGCAUAGUCCAGGG AGUGGCGAAAGUCACACAAACCGG	25
D37-4	GUGCCUUGCGCCGGGAAACCACGCAAGGGAUGGUGUCAAAUUCGGUGAAACCUAAGCG CCCGCCCGGGCGUACGGCUACGCCGAGCCAAGCUUCGGCGCCUGCGCCGAUGAAAGUGU AGAGACUAGACGGCACCCACCUAUGGCAAACGCUAUGGUGAAGGCUUAGUCCAGGGUG UGGCGAAAGUCACACAAACCGG	2
D37-10	GUGCCUUGCGCCGGGAAACCACGCAAGGGAUGGUGUCAAAUUCGGCGAAACCUAAGCG CCCGCCCGGGCGUAAGGCAACGCCGAGCCAAGCUUCGGCGCCUGUGCCGGUGAAGGUG UAGAGACUAGACGGCCCCCACCUAAGGCAACCGCUAUGGUGAAGGCAUAGUCCAGGGA GUGGCGAAAGUCACACAAACCGG	2
D38-11	GUGCCUUGCGCCGGGAAACCACGCAAGGGAUGGUGUCAAAUUCGGCGAAACCUAAGCG CCCUACCGGGCGUAUGGCAACGCCGAGCCAAGCAUCGGCGCCUGCGCCGAUGAAUGUGU AGAGACUAGACGGCACCCACCUAAGGCAAACGCUAUGGUGAUGGCAUAGUCCAGGGAG UGGCGAAAGUCACACAAACCGG	2
D38-13	GUGCCUUGCGCCGGGAAACCACGCAAGGGAUGGUGUCAAAUUCGGCGAAACCUAAGCG CCUACCCGGGCGUACGGCAACGCCGAGCCAAGCUUCGGCGCCUGCGCCGAAGAAUGUGU AGAGACUAGACGGCACCCACCUAAGGCAAACGCUAUGGUGAAGGCAUAGUCCAGGGAG UGGCGAAAGUCACACAAACCGG	2
D45-5	GUGCCUUGCGCCGGGAAACCACGCAAGGGAUGGUGUCAAAUUCGGCGAAACCUAAGCG CCCGCCCGGGCGUAUGGCAACGCCGAGCCAAGCUUCGGCGCCUGCGCCGAUGAAGGUGU AGAGACUAGACGGCACCCACCUAAGGCGAACGCUAUGGUGAAGGCAUAGUCCAGGGAG CGGCGAAAGUCACACAAACCGG	2

Table S1 **Sequences used to study magnesium induced structural variation.** The 'Sequence' column contains the sequence of the RNA used for activity assays (Fig. S5) and SHAPE analysis (Fig. S6 and Fig. S7). Sequence data was obtained by Sanger sequencing from RT-PCR products, and mutations were detected by pairwise alignment to the wild-type *Azoarcus* ribozyme sequence (LastZ). Mutations are indicated as red letters (SNPs and insertions) or "-" (deletion). The 'Seq ID' column is an experimental reference, and has no meaning other than to identify the specific sequence. The 'Selection [Mg^{2+}]' column indicates under which concentration of magnesium the sequence was selected.

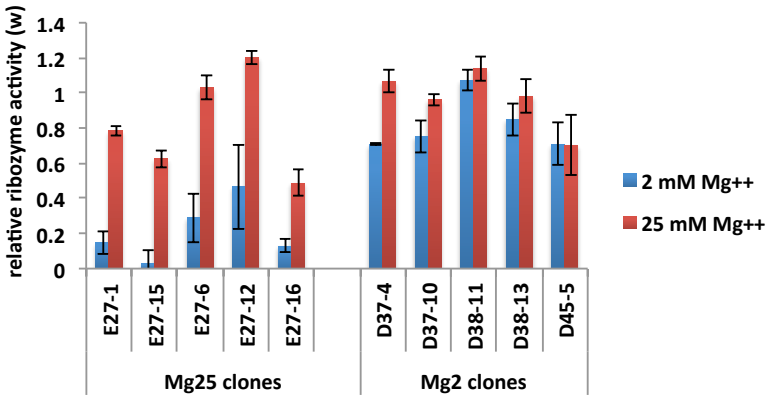

Figure S5 **Magnesium dependence of ribozyme activities of sampled clones.** Individual RNA molecules that were the source of the RNA SHAPE data were assayed for the native ribozyme activity (reverse splicing). Reactions were carried out under the same conditions as the selections (1h, 25 µM RNA substrate, and indicated Mg^{2+} concentration). Reacted and unreacted molecules were separated by denaturing PAGE (6% polyacrylamide, 8M urea) followed by fluorescent staining with GelRed (Biotium). Activity was quantified as the fraction of total fluorescence in the reacted band, after background subtraction. Values represent the average of two measurements, with error bars representing standard error of the mean.

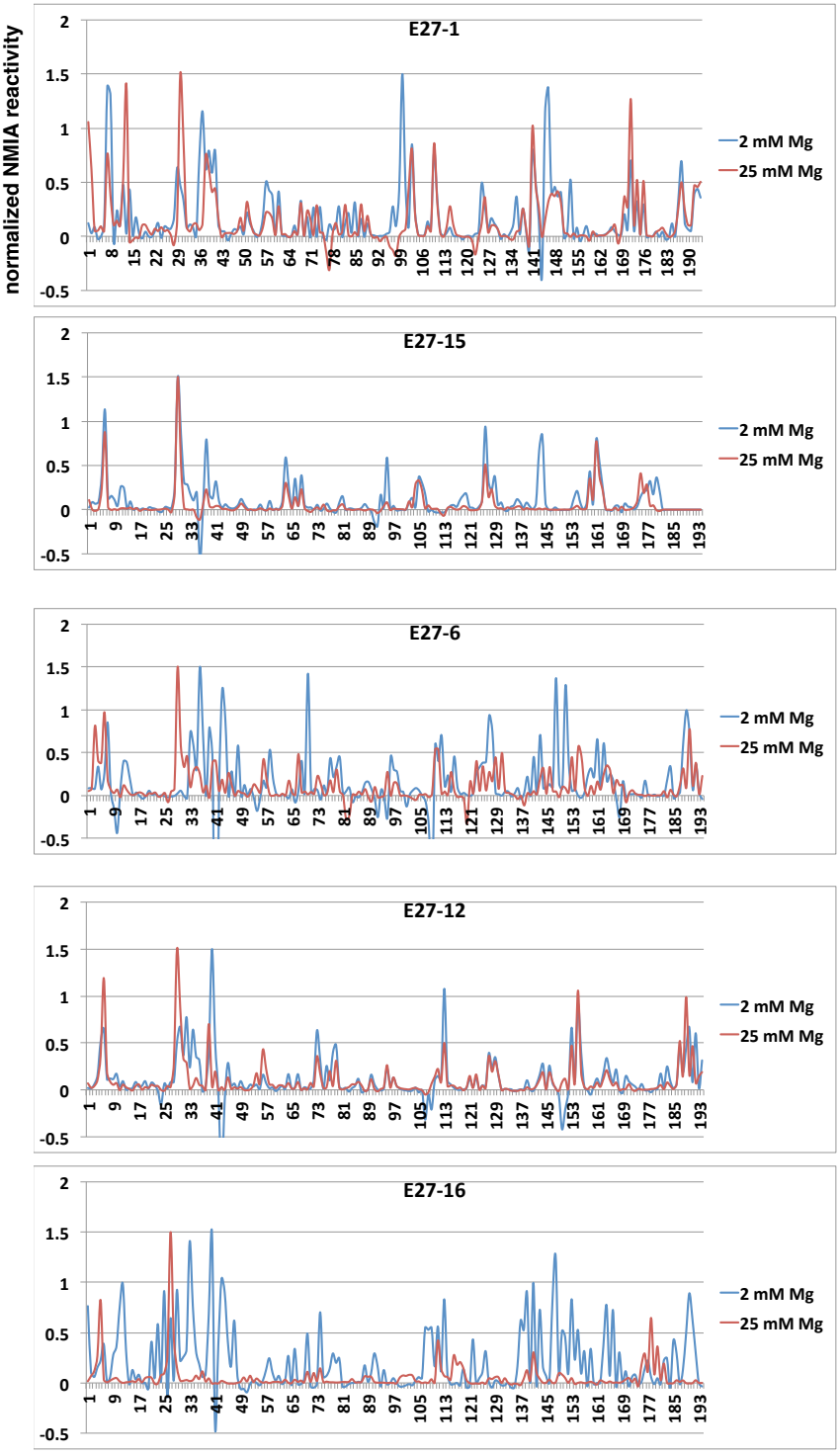

Figure S6 **RNA SHAPE analysis for individual RNA molecules that survived selection at 25 mM Mg^{2+}.** Traces show the nucleotide position on the x-axis and NMIA reactivities on the y-axis. Each plot contains data for the same RNA preparation folded at either 25 mM Mg^{2+} (red) or 2 mM Mg^{2+} (blue). Experiments were conducted side by side to minimize variation. The same ddATP ladder was premixed prior to capillary electrophoresis. Data was aligned with the program QuShape, with the maximum value normalized to 1.5.

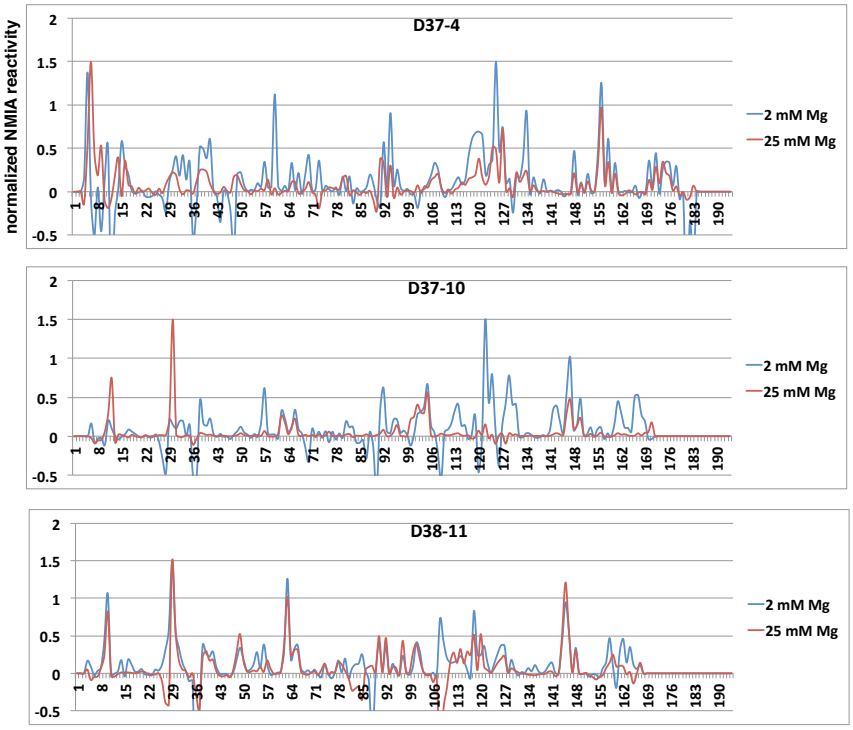

Figure S7 **RNA SHAPE analysis for individual RNA molecules that survived selection at 2 mM Mg^{2+}.** Traces show the nucleotide position on the x-axis and NMIA reactivities on the y-axis. Each plot contains data for the same RNA preparation folded at either 25 mM Mg^{2+} (red) or 2 mM Mg^{2+} (blue). Data was aligned with the program QuShape, and normalized to maximum values of 1.5.

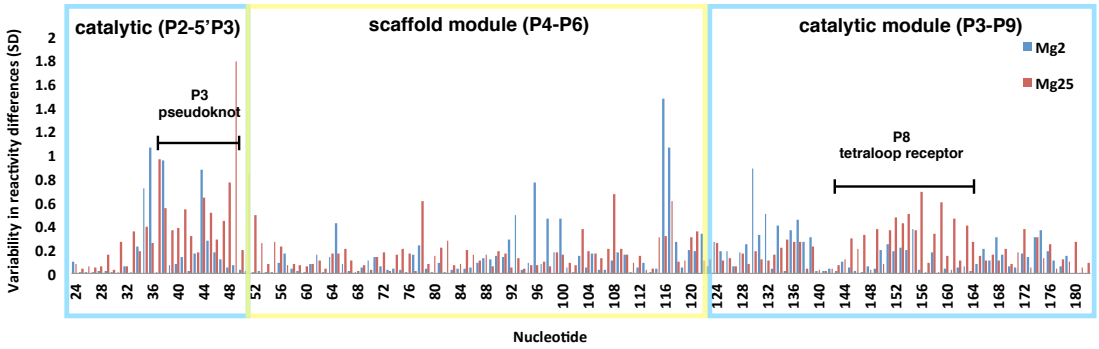

Figure S8 **Per nucleotide structural variability of clones analyzed by SHAPE.** Variability of the magnesium-induced differences in NMIA reactivity at each nucleotide position is shown. Each bar represents the standard deviation of the reactivity differences observed at that nucleotide position for the ribozyme variants selected at either 25 mM Mg^{2+} (blue) or 2 mM Mg^{2+} (red). Black bars indicate two regions in the catalytic module that contribute to higher variability in the catalytic module of the Mg25 clones. The nucleotides of the catalytic modules show 24% higher standard deviation in the Mg25 clones (SD=3.54) relative to the Mg2 clones (SD=2.85). The nucleotides of the scaffold module shows 9.2% lower standard deviation in the Mg25 clones (SD=1.98) than in the Mg2 clones (SD=2.18).

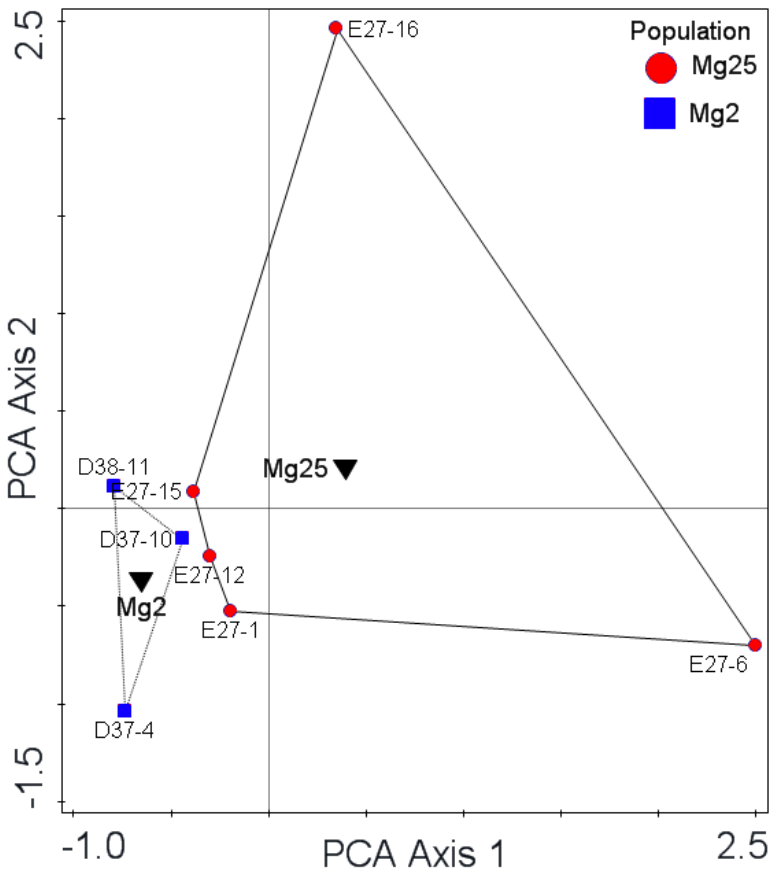

Figure S9 **Analysis of the amount of variation in RNA structure induced by altering magnesium concentration.** Principle component analysis (PCA) of the differences in NMIA reactivities at 25 mM and 2 mM Mg^{2+}. From each plot in Fig. S5 and S6, the difference between the red and blue trace at each nucleotide position was determined. The PCA summarizes the variation in these differences between the clones from each population, from the most informative two-dimensional perspective. The two most informative components are shown above, and combined they account for 53.2% of the variance (PCA Axis 1, 34.7%; PCA Axis 2, 18.5%). The black triangles show the centroid of each sample. "Mg25" are clones that survived selection at 25 mM Mg^{2+}, and "Mg2" are clones that survived selection at 2 mM Mg^{2+}. The size of the polygon connecting the data points from each sample illustrates the amount of variation in RNA structure induced by altering Mg^{2+} concentration (25 mM vs. 2 mM Mg^{2+}) as determined by SHAPE analysis with NMIA (see Fig. S5 and S6 for source data).

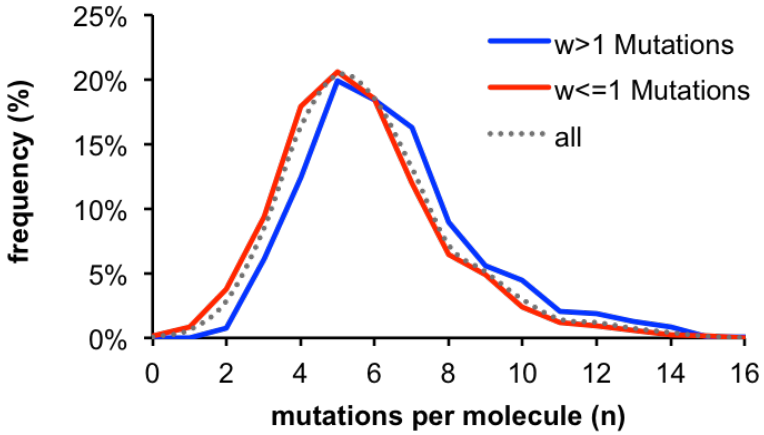

Figure S10 **Sequences with specific mutations in the scaffold contain one extra mutation on average.** Mutations per molecule (n) were determined by pairwise alignment to the wild-type ribozyme sequence. The frequency of molecules with a given number of mutations was determined for the molecules that survived selection at 25 mM Mg^{2+} (i.e. Fig. 2D, main text). Here, this population was bioinformatically parsed into two samples: those that contain mutations that show fitness effect $w > 1$ (blue), and the rest of the molecules ($w \leq 1$, red). The sequences that make up the blue distribution have on average approximately one more mutation per molecule (generalized linear model, p<2e-16, n=3364).

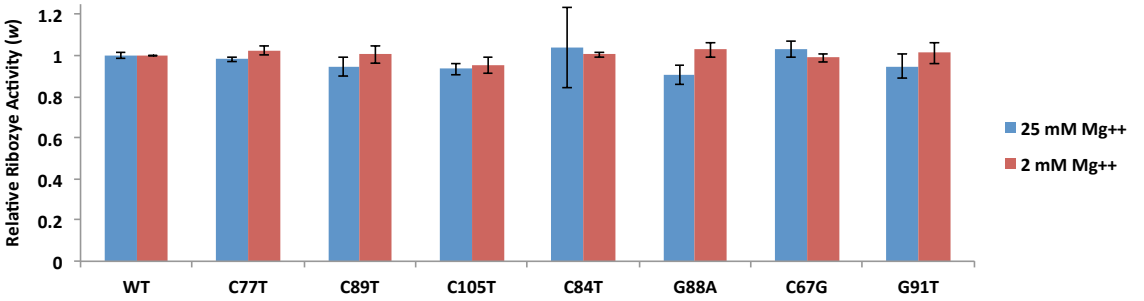

Figure S11 **Functional consequence of specific mutations located in the scaffold module.** Several of the mutations with fitness effects $w > 1$ at 25 mM Mg, based on frequencies observed in the sequence data (Fig. 2A), were assayed for their effect on the native ribozyme activity. Each ribozyme sequence with the above individual mutation, in the otherwise wild-type background, was purchased as a chemically synthesized oligonucleotide (IDT). These oligos were amplified by PCR to introduce the promoter for T7 RNA polymerase. Mutations were confirmed by Sanger sequencing. RNA was produced by transcription with T7 RNA polymerase. Ribozyme Activity (w) is reported relative to the wild-type Azoarcus ribozyme (WT) in either 25 mM Mg^{2+} or 2 mM Mg^{2+}. Reaction conditions were the same as used in the selection experiments, and for population fitness measurements (Materials and Methods, main text). Mutations are indicated below each bar graph as 'XNY', where 'X' indicates the nucleobase in the wild-type sequence, 'N' indicates the position of the mutations in the ribozyme sequence (numbered according the Fig. 1), and 'Y' indicates the mutant nucleobase introduced into the variant. Values represent the average of two measurements with bars representing standard error.

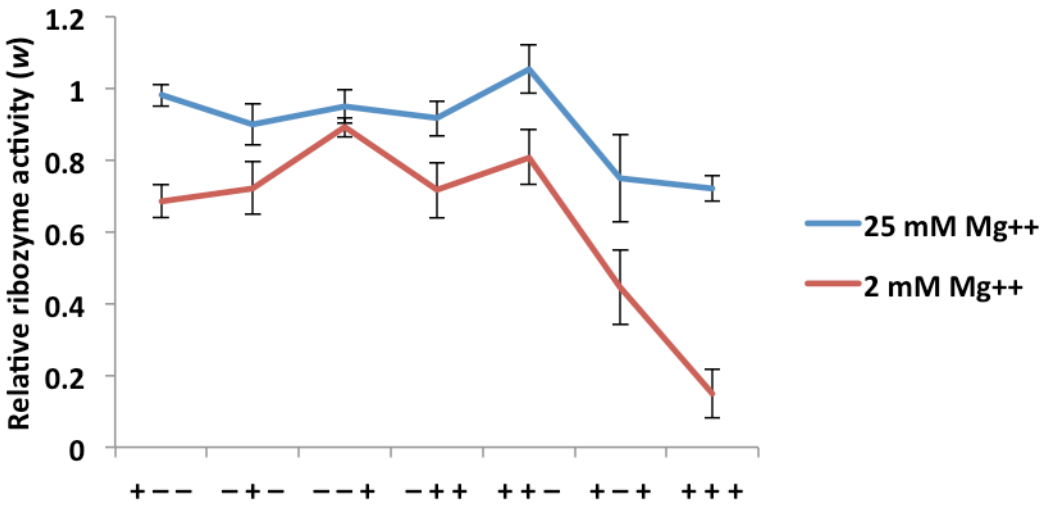

Figure S12 **Ribozyme activity effects of a series of scaffold and catalytic module mutations.** Ribozyme activities were determined for all combinations of the three mutations found in clone E27-1 (Table S1), and compared to the activity of the wild-type ribozyme under the same conditions. The three +/- positions of each categorical label on the x-axis refer to the presence (+) or absence (-) of the three mutations C90A, A128C , and C177T, respectively. For example, '+ + +' = triple mutant with all three mutations; '- + +' = a double mutant, with A128C and C177T. The mutation C90A is in the scaffold module, while A128C and C177T are found in the catalytic module. Data points represent the mean of two measurements, and error bars show standard error of the mean.

Supporting Results and Discussion

We used chemical probing to analyze the non-native structures produced under environmental stress (2 mM $MgCl_2$). We used an experimental protocol referred to as RNA SHAPE (Selective 2'-Hydroxyl Acylation analyzed by Polymerase Extension). The experiments involve folding the RNA molecule under specific salt conditions (i.e. 2 mM or 25 mM $MgCl_2$), and then treating the RNA with a chemical (NMIA) that reacts with 2'-OH residues in a way that depends on structural context in the following way. Nucleotides involved in secondary or tertiary contacts are less flexible, and they react less with the chemical reagent. Unstructured nucleotides are more flexible, and react more with the chemical reagent. Each position is assigned a "reactivity" which reports on the structural context of the nucleotide. We utilized a published protocol that uses fluorescently labeled primers for reverse transcription followed by separation by capillary electrophoresis. Data was analyzed with the software package QuShape which "enables efficient, reliable, highly automated, and accurate analysis of high-throughput capillary electrophoresis-detected nucleic acid chemical probing experiments" (http://www.chem.unc.edu/rna/qushape/).

Based on our capacitance hypothesis, we predicted that RNA molecules selected under relaxed conditions (25 mM $MgCl_2$) would show a higher structural *variability* under the environmental stress of low magnesium than would the RNA molecules selected under this low magnesium condition. This is because the "Mg25" population contains cryptic mutations, and the greater genetic variation would produce greater structural variation when revealed under stressful conditions. We therefore conducted RNA SHAPE experiments with RNA folded at both 25 mM and 2 mM Mg for several randomly selected clones from both populations (Fig. S6 and Fig. S7).

To quantify the *change* in structures induced at low magnesium, we determined the *difference* in NMIA reactivity for each RNA sequence, by subtracting the two data sets in each plot of Fig S6 and Fig. S7. This data reports on the amount of structural difference at each nucleotide position caused by changing magnesium concentration. We next estimated the variety of structures revealed at low magnesium. For this, we calculated the standard deviation in reactivity differences at each nucleotide position within the clones from each population, separately (Fig. S8). The bars in Fig. S8 represent the standard deviation in the NMIA differences at that position between clones from either population.

To illustrate the variance in the SHAPE data of each population induced by low magnesium, we next turned to a principle component analysis (PCA) of the per nucleotide reactivity differences (Fig. S9). The PCA illustrates the greater variance in the reactivity differences of the molecules surviving under *relaxed* selection (Mg25) conditions when exposed to the *stressful* condition of low magnesium. Further, we determined descriptive statistics of these differences in the context of each module of the structure. Importantly, we find that the catalytic modules from the Mg25 population show a 24% higher standard deviation in the NMIA reactivity differences between 25 mM and 2 mM Mg^{++}, as compared to the catalytic modules from the Mg2 population. In contrast, the scaffold module shows a 9% lower standard deviation in the Mg25 population. Importantly, these results illustrate that while cryptic mutations were harbored in the scaffold module (main text, Fig. 2A and Fig. 2B), the structural variability caused by unfolding occurs primarily in the catalytic module. Two tertiary structural elements in the catalytic module (P3 pseudoknot and P8 tetraloop receptor) in particular appear to be the main contributor to this increased variability, and they are labeled with black bars in Fig. S9. This data is in support of our conclusion that the modular structure facilitates phenotypic capacitance. The data in Fig. S12 provide further support for our conclusion. This data shows the magnesium sensitivity for a ribozyme sequence selected at 25 mM Mg^{++}, which contains three mutations relative to

the wild-type ribozyme; one in the scaffold module and two in the catalytic module. The data show that the two catalytic module mutations, individually (*–+–*, *––+*) or in combination (*–++*), only contribute slightly to the magnesium sensitivity. However, with the addition of the scaffold mutation, when all three mutations are combined (*+++*), the full magnesium sensitivity is revealed (see red vs. blue data in Fig. S12, x-axis label "+++"). We conclude that this mutated scaffold module can perform its function at high magnesium, maintaining the normal ribozyme phenotype. However, at low magnesium, the scaffolding function fails, revealing the tendency of the mutated catalytic module to misfold.